Modes of spheroidal ion plasmas at the Brillouin limit

M. D. Tinkle, R. G. Greaves, and C. M. Surko
Department of Physics, University of California, San Diego, La Jolla, California 92093

(Received 28 July 1995; accepted 27 October 1995)

The confinement properties and collective modes of single-component plasmas are investigated in a quadrupole Penning trap. Brillouin-density pure ion plasmas are generated by electron-beam ionization of a low-pressure gas. Large, spheroidal, steady-state plasmas are produced, extending out to contact one or more of the trap electrodes. With the density fixed at the Brillouin limit by the high ion production rate, the electrode potentials determine the plasma shape. The frequencies of azimuthally propagating cyclotron and diocotron modes are found to vary significantly with the plasma aspect ratio. For oblate plasmas, the frequencies are in good agreement with a simple fluid model. © *1996 American Institute of Physics.* [S1070-664X(96)02202-5]

I. INTRODUCTION

The properties of single-component plasmas in Penning traps are of fundamental interest, and they have been the subject of numerous experimental and theoretical studies.[1–4] Axial confinement in such plasmas is provided by an electrostatic potential well, while radial confinement is provided by a magnetic field. However, if the plasma density rises above a critical value, the repulsive and centrifugal forces on the rotating plasma can no longer be balanced by the force due to the confining magnetic field. This density limit—the Brillouin limit—was first described in the context of electron beams,[5] but it applies equally to plasmas in Penning traps. For non-relativistic plasmas, this limit is far more restrictive than the analogous limit for neutral plasmas (i.e., $\beta \leqslant 1$, where β is the ratio of plasma pressure to magnetic field pressure), and it is also much less than the present practical limit for tokamaks ($\beta \simeq 5\%$). A unique feature of plasmas at the Brillouin limit is that the effective magnetic field vanishes, and the plasmas behave as though they are electrostatically confined. In the reference frame rotating with the plasma, particles execute straight-line orbits in the interior of the plasma, and are then reflected by the sheath at the plasma boundary.[1,2] Plasmas at the Brillouin limit have been studied as beams[6] and drifting plasmas,[7] but there have been only a few reports relating to trapped plasmas.[8]

In addition to its basic interest, the Brillouin limit represents a restriction on many technological applications where single-component plasmas are required at the highest possible density. For example, it represents a stringent limitation on alternative fusion energy concepts based on Penning traps, and significant theoretical and experimental efforts have recently been directed at developing techniques for exceeding the Brillouin limit.[9–12] Dense trapped plasmas are now being developed as targets for high-energy beam experiments,[13] and such plasmas have also been used as focussing elements for high-energy beams.[14] Dense ion plasmas are being investigated as a method of trapping and cooling positrons for the production of low-emittance beams.[15] For these experiments, the Brillouin limit restricts the choice of ions to the lighter species. Finally, the Brillouin limit places a practical restriction on the accumulation of antiprotons[16–18] for the production of antihydrogen.[19]

There have been relatively few experiments on confined Brillouin-density plasmas, because most non-neutral plasma experiments have been performed with pure electron plasmas, in which the density limit is typically quite high. An experiment by Dimonte[7] demonstrated a Brillouin-density Li^+ ion plasma produced by a relatively simple source. Most ion plasma devices, however, are designed for use with laser-induced fluorescence diagnostics in high magnetic fields and do not naturally generate plasmas at the Brillouin limit. Through the application of laser torques, microplasmas consisting of about 10^5 ions have been compressed to the Brillouin limit,[20] and properties of collective modes in these plasmas have been studied.[8,20]

Single-component plasmas support a wide variety of collective modes, many of which are similar to those found in neutral plasmas. These modes include axial space-charge waves such as the Trivelpiece-Gould mode,[7,21,22] purely azimuthal modes such as the diocotron and cyclotron modes, and ''tilted'' modes where the plasma motion is both axial and azimuthal.[23] Diocotron modes have frequencies near multiples of the rotation frequency, which in most experiments is in the range of a few kilohertz to a few hundred kilohertz. Because such frequencies are convenient from an experimental point of view, these modes have received the most attention in pure electron plasmas.[24–29] Cyclotron modes have frequencies near multiples of the cyclotron frequency, $\Omega_c = qB/Mc$, where B is the magnetic field, c is the speed of light, and q and M are the charge and mass of the plasma particles, respectively. For electron plasmas, the cyclotron frequency is inconveniently high (in the range of a few hundred to a few thousand megahertz for an adequate confining magnetic field) and cyclotron modes in pure electron plasmas were not studied until the recent experiments by Gould and LaPointe,[30,31] in a device specifically designed to operate at these frequencies. In that experiment, a family of radially trapped Bernstein modes was observed, with mode spacing determined by the electron temperature. In ion plasmas, the cyclotron frequency again falls in the experimentally convenient range of a few tens of kilohertz to a few thousand kilohertz, and recently these modes have been investigated in multispecies ion plasmas.[32] In this latter experiment, frequency shifts in the cyclotron modes were ob-

served, which were quantitatively explained by a multifluid cold-plasma theory.

We have developed a new steady-state mode of operation of a quadrupole trap that enables us to explore a range of plasma phenomena including plasma confinement and cyclotron and diocotron modes in pure ion plasmas near the Brillouin density.[33,34] The technique releases ions continuously into the plasma by ionizing a background gas using an electron beam. Because the ion confinement is relatively good, the plasma quickly reaches the Brillouin limit, where it can be sustained in a steady-state condition. The technique is convenient in that it can be easily applied to a variety of ion species, simply by changing the background gas, thus permitting the exploration of mass dependences. The present experiments complement the plasma mode studies carried out in precision quadrupole traps,[8,35] in that a different family of modes is studied in plasmas that are hotter and much larger than those in the quadrupole traps. The mode frequencies we observe are well described by the same cold fluid theory[36] that was developed for the microplasmas.

The ion cyclotron resonance is the basis of the most precise technique for mass spectrometry available.[37] Although the technique is generally applied to small numbers of particles that are not in a plasma state, space charge effects can play an important role by shifting the resonant frequency.[37,38] A quantitative understanding of the effects of plasma density on the collective modes could lead to the ability to utilize the larger signals available from dense plasmas in making precision ion mass measurements.

Plasma modes can also provide diagnostic information. For example, the diocotron mode frequency of a cylindrical plasma is often used to obtain the line charge density.[3] In spheroidal plasma the analytical theory of Dubin,[23,36] which comprehensively describes all the cold-fluid modes of spheroidal plasmas in Penning traps, provides the basis for the measurement of aspect ratio and density.[20,39] Temperature effects lead to a deviation from the cold-fluid model,[23] and this enables the temperature to be measured by measuring mode frequencies.[40] The mode frequencies of the higher-order diocotron and cyclotron branches in spheroidal plasmas have also been predicted to depend on aspect ratio,[36] and could lead to a supplemental or alternative diagnostic. These types of non-destructive diagnostics are expected to be particularly important for monitoring the antimatter plasmas now under study.[15,17,18,41,42]

The remainder of this paper is structured as follows. In Sec. II, we review the confinement properties of plasmas in quadrupole traps, and present our model for plasma confinement at the Brillouin limit. In Sec. III we describe the experiment. In Sec. IV, we present the experimental data and a comparison with theory. We then discuss the results and summarize the paper in Sec. V.

II. ION CONFINEMENT IN A QUADRUPOLE TRAP

A. Critical voltage

An ideal quadrupole Penning trap consists of a uniform magnetic field, B, directed along the z axis and an electrostatic potential of the form

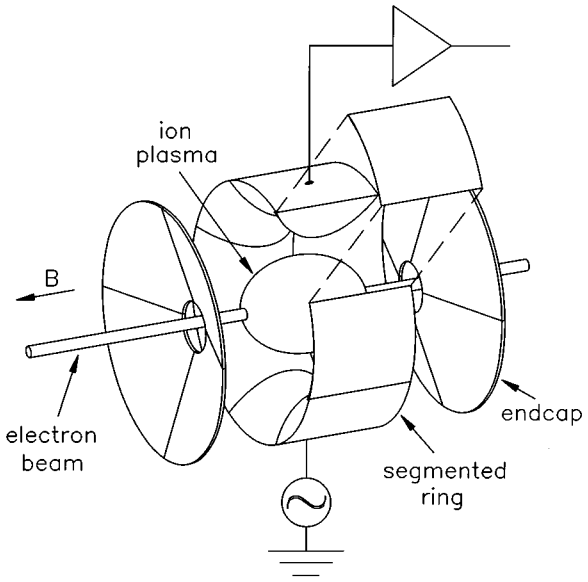

FIG. 1. Exploded schematic of the ion plasma experiment, showing the electron beam, the spheroidal ion plasma, and the electronics used for mode excitation and detection.

$$\Phi(\rho,z)=\frac{V}{z_0^2}\left(z^2-\frac{1}{2}\rho^2\right),$$

where $\rho=(x^2+y^2)^{1/2}$ is the cylindrical radius and V and z_0 are constants. This potential is often realized by machining electrodes to approximate the hyperboloidal equipotential surfaces defined by the equation

$$z^2-\frac{1}{2}\rho^2=\pm z_0^2,$$

and biasing them to potentials $\pm V$. The result is a pair of mirror-symmetric ''endcaps'' biased at a potential V and a ''ring'' electrode biased at a potential $-V$. The trap used in these experiments, shown schematically in Fig. 1, is an approximation to such a trap, with a scale parameter $z_0=6.3$ cm. For this geometry, the distance to the endcaps from the center of the trap is z_0, and $\rho_0=\sqrt{2}z_0$ is the inner radius of the ring electrode. Another technique for obtaining a quadrupole potential, at least over some volume of the trap, is to use cylindrical electrodes with specially chosen lengths and potentials—the ''orthogonalized'' cylindrical Penning trap.[43] This technique can be applied equally to a geometry with open or closed endcaps.

A single trapped ion executes simple harmonic oscillations along the z direction at a frequency

$$\omega_z=\left(\frac{2qV}{Mz_0^2}\right)^{1/2}.$$

The motion in the x and y coordinates consists of a rapid circular cyclotron motion at a frequency

$$\Omega_c'=\frac{\Omega_c}{2}+\frac{1}{2}\sqrt{\Omega_c^2-2\omega_z^2}, \tag{1}$$

accompanied by a slower circular drift around the z axis at the magnetron frequency,

$$\Omega_M=\frac{\Omega_c}{2}-\frac{1}{2}\sqrt{\Omega_c^2-2\omega_z^2}, \tag{2}$$

where Ω_c is the cyclotron frequency in the absence of the trap electric field. The amplitudes and phases of the three independent oscillations may be determined from the initial conditions. For example, the radius of the cyclotron motion is

$$\rho_c=\left[\frac{\dot{\rho}^2+\rho^2(\dot{\phi}+\Omega_M)^2}{\Omega_c^2-2\omega_z^2}\right]^{1/2}, \tag{3}$$

where ρ is the radial position and $\dot{\rho}$ and $\rho\dot{\phi}$ are the radial and azimuthal components of the particle velocity. The radius, ρ_d, of the magnetron drift motion is found from the same formula by replacing Ω_M with Ω_c'.

The confined particle orbits described above are only possible when $\omega_z^2<\Omega_c^2/2$; for higher values of ω_z, the particle trajectories in x and y are combinations of hyperbolic sine and cosine functions, and the particle will strike the ring electrode quickly. As a result, V must be kept below a critical value,

$$V_c=\frac{B^2z_0^2q}{4Mc^2}, \tag{4}$$

for the trap to work. Conversely, for a particular choice of V and B, only particles with $M/q<B^2z_0^2/Vc^2$ will be confined.

B. Spheroidal equilibrium

The thermal equilibrium of a large number of particles confined in a quadrupole Penning trap at a low temperature is a uniform-density spheroidal plasma, rotating rigidly.[44] The rotation frequency, ω_r, satisfies the same equation found for cylindrical plasmas,

$$\omega_p^2=2\omega_r(\Omega_c-\omega_r), \tag{5}$$

where $\omega_p=(4\pi q^2n/M)^{1/2}$ is the plasma frequency, and n is the number density of the plasma. The spheroids are biaxial ellipsoids with rotational symmetry about the z axis, so they are completely specified by their length, L, along the z axis and their radius, r_p, at $z=0$. The ratio of length to diameter,

$$\alpha=\frac{L}{2r_p}, \tag{6}$$

is referred to as the aspect ratio. In equilibrium, α is related to the plasma density by the equation[36]

$$\omega_p^2=\omega_z^2\frac{2}{A_3(\alpha)}, \tag{7}$$

where

$$A_3(\alpha)=\frac{2Q_1^0[\alpha(\alpha^2-1)^{-1/2}]}{\alpha^2-1}, \tag{8}$$

and Q_1^0 is a Legendre function of the second kind. The plasma frequency is a monotonically increasing function of α which approaches its minimum value, $\omega_p=\omega_z$, as $\alpha\to 0$.

C. Brillouin limit

As in the cylindrical plasma equilibrium, the radial electric field inside the plasma is proportional to ρ, having the form $E_\rho=M\omega_p^2\rho/2qz_0^2$. Comparing this with the radial electric field of the trap, $E_\rho=M\omega_z^2\rho/2qz_0^2$, which led to the condition $\omega_z^2<\Omega_c^2/2$, it is clear that a similar condition applies to the plasma frequency. Just as the trap field prevents confinement for $V\geqslant V_c$, plasma self-fields limit the density of trapped particles to the Brillouin density,[5]

$$n_{\mathrm{B}}=\frac{B^2}{8\pi Mc^2}, \tag{9}$$

at which $\omega_p^2=\Omega_c^2/2$. At this limiting density, the plasma rotation frequency is $\omega_r=\Omega_c/2$, and the plasma has the highest aspect ratio available for the specified values of ω_z and Ω_c.

In a plasma, particles move at nearly constant velocities in the z direction and reflect from the plasma boundary, rather than undergoing simple harmonic oscillation. There is a distribution of axial bounce periods determined from the plasma temperature, as in cylindrical plasmas, and from the particle radius. The motions in x and y are similar to those described above for single trapped particles, with the simple change $\omega_z\to\omega_p$ in Eq. (1), Eq. (2), and Eq. (3), except that motions in the plasma boundary are more complicated. As the Brillouin limit is approached ($\omega_p\to\Omega_c/\sqrt{2}$), the orbit size of the plasma particles diverges, just as the orbit size of single trapped particles diverges when the confinement limit is approached ($\omega_z\to\Omega_c/\sqrt{2}$). In this case, however, particles may remain confined in the trap as long as the plasma boundary is well separated from the electrode surfaces, because their orbit radius becomes finite once they leave the plasma. If the Brillouin limit is exceeded, the plasma will expand across the magnetic field until the density is reduced to $n=n_B$. In the limit of high magnetic field or low temperature, the particle motions in a plasma at the Brillouin density limit are straight-line trajectories followed by specular reflections from the plasma boundary, when viewed in a frame rotating with the plasma.

D. Brillouin spheroid model

The Brillouin density for argon ions in a magnetic field of 1 kG is $n_{\mathrm{B}}=6.63\times10^5\ \mathrm{cm}^{-3}$. Small numbers of ions in our trap have a confinement time of the order of 1 s at a neutral gas pressure of 10^{-6} Torr. As described in more detail in Sec. III, we can fill the trap by ionizing the background gas using an electron beam. Therefore, if ions are released into the trap at a rate greater than $10^8\ \mathrm{cm}^{-3}\ \mathrm{s}^{-1}$, the density will approach the Brillouin limit in a matter of milliseconds, unless space charge is sufficient to allow ions to escape through the endcaps. This latter possibility will occur for low confining potentials. We can estimate the minimum value of V required to prevent such a loss by considering a spheroidal equilibrium plasma with the diameter of the electron beam, the length of the trap, and the Brillouin density. The value of V for which this equilibrium is obtained is found from Eq. (7), which may be written as

$$V=A_3(\alpha)\pi z_0^2qn, \tag{10}$$

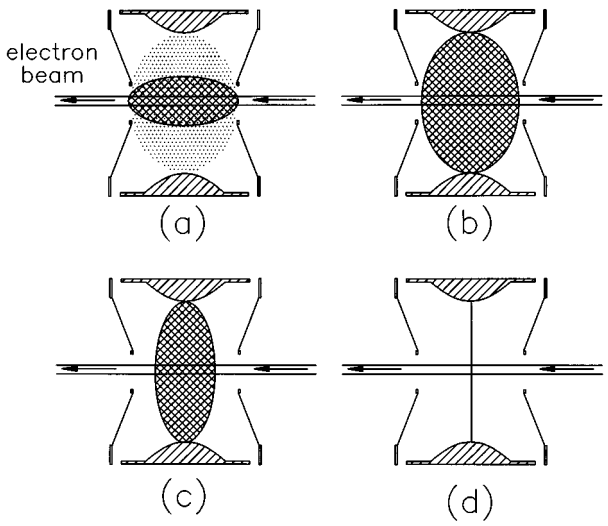

FIG. 2. Model of the steady-state ion plasma for (a): $V_{\min}<V<V_t$, endcap-limited plasma (crosshatched) with halo (dotted), $\alpha>1/\sqrt{2}$; (b) $V=V_t$, transition plasma, $\alpha=1/\sqrt{2}$; (c) $V_t<V<V_c$, ring-limited plasma, $\alpha<1/\sqrt{2}$; and (d) $V=V_c$, disk plasma, $\alpha=0$. For $V>V_c$, there is no plasma.

by setting $n=n_B$ and $\alpha=z_0/r_{\text{beam}}$, where r_{beam} is the radius of the electron beam. For argon ions in a magnetic field of 1 kG, the result is $V_{\min}=0.45$ V. By contrast, for an electron plasma of the same diameter as the electron beam to have the Brillouin density would require a confinement voltage greater than 30 kV.

For the ion plasmas we have studied, $V>V_{\min}$, so charge is not expected to escape along the trap axis before the Brillouin density is reached. Radial transport due to gas scattering will be minor on the millisecond time-scale, but once the Brillouin density is reached, the addition of more ions will cause immediate expansion due to the loss of radial force balance. The ion distribution that evolves as ions are continually added is probably not a true thermal equilibrium, but because of the nearly unmagnetized nature of the interior of these high-density plasmas, it may be reasonable to assume that the force balance achieved in equilibrium is approximately attained by these plasmas. The data presented in Sec. IV support the contention that the plasmas formed in steady state may be adequately described as Brillouin-density spheroids with aspect ratios determined by the cold fluid equilibrium [Eq. (10)].

With the aspect ratio determined by the Brillouin density and the confining voltage V according to Eq. (10), the remaining ingredient of the model is the plasma size. With ions being continually produced, the plasma will grow in size (maintaining a fixed aspect ratio) until it contacts one of the electrodes, after which additional ions formed will flow to that electrode, and a steady state will be established. For a fixed value of B, the aspect ratio varies with V, with increasing values of V leading to increasingly oblate spheroids. Therefore, for low values of V, the plasma touches the endcaps, as shown in Fig. 2(a), while for large values of V, it touches the ring electrode, as shown in Fig. 2(c). A plasma with an aspect ratio of $\alpha=1/\sqrt{2}$ has the right shape to touch both the endcaps and the ring electrode, giving it a volume of about 2×10^3 cm^3, the largest spheroidal plasma that may be confined in this trap. This case is illustrated in Fig. 2(b). The confinement voltage, V_t, that results in this shape for a Brillouin-density plasma has a prominent role in the experiment; it may be derived as follows. Assume $n=n_B$ and $\alpha=1/\sqrt{2}$ and solve for V in Eq. (10) to find $V_t=A_3(1/\sqrt{2})/2\cdot[B^2z_0^2q/4Mc^2]$. Then from Eq. (8), $A_3(1/\sqrt{2})=-4Q_1^0(-i)=4-\pi$, and the term in brackets is [from Eq. (4)] the critical voltage V_c, so we have the simple result

$$V_t=(2-\pi/2)V_c. \tag{11}$$

For $V<V_t$, the plasma length is fixed at $L=2z_0$, and excess ions leave through the endcaps. Due to collisions with neutral gas atoms, some particles will be transported radially out of the Brillouin-density core and will diffuse to the ring electrode. Our inference is that they form a tenuous halo plasma surrounding the core, as shown in Fig. 2(a). For $V>V_t$, the plasma radius is fixed at $r_p=\rho_0$, and there is no halo plasma. As $V\to V_c$, the plasma length tends to zero, as shown in Fig. 2(d).

III. DESCRIPTION OF THE EXPERIMENT

The experiments were performed in a Penning trap designed to accumulate and store low-energy positrons.[41,42] A magnetic field of up to 1.3 kG is aligned with the electrode structure shown in Fig. 1, which approximates the hyperboloidal electrodes of a precision quadrupole trap. The ring electrode is split azimuthally into eight sectors.

Ions are formed by passing an electron beam along the axis of the trap, as shown schematically in Fig. 1. The rate at which ions are formed inside the trap is approximately

$$\frac{dN_{\text{ion}}}{dt}\simeq\frac{2z_0n_n\sigma_iI_{\text{beam}}}{e}, \tag{12}$$

where σ_i is the ionization cross-section, n_n is the density of neutral gas atoms, I_{beam} is the beam current, and $2z_0$ is the distance between the endcaps along the trap axis. This ignores the variation of the beam energy inside the trap, which could be included by using an averaged value of σ_i. Ionization cross-sections typically rise rapidly as the beam energy is increased above the first ionization threshold, E_I, and reach a maximum value, $\sigma_{\max}$, at a beam energy on the order of 100 eV. For argon, $E_I=15.8$ eV and $\sigma_{\max}\simeq4\times10^{-16}$ cm^2 occurs at a beam energy of 90 eV. As described below, the beam energy is kept below the second ionization energy threshold (i.e., 43.4 eV for argon), at which energy, $\sigma_i\simeq\sigma_{\max}/2$:

$$\frac{dN_{Ar^+}}{dt}\simeq0.5\times10^8\ \text{s}^{-1}\cdot pI_{\text{beam}}, \tag{13}$$

where the beam current is expressed in microamps and the gas pressure, p, is in microtorr.

The electron beam is emitted from the circular oxide-coated cathode of an electron gun with radius $r_g=0.7$ cm in a magnetic field $B_g=150$ G. Its radius as it passes through the trap will depend on the trap magnetic field:

$$r_{\text{beam}}=r_g\sqrt{B_g/B}. \tag{14}$$

Thus the density of ion production is

$$\frac{dn}{dt} \simeq \frac{dN_{\text{ion}}}{dt} \frac{B}{2\pi r_g^2 z_0 B_g}, \tag{15}$$

or about 2×10^8 cm^{-3} s^{-1} for a one microamp beam passing through 10^{-6} Torr of argon in a magnetic field of one kilogauss.

As with other sources of pure ion plasmas, production of doubly ionized particles is a concern. Again taking the example of argon, above the second ionization threshold energy, E_{II}=43.4 eV, Ar^{++} ions are formed from gas atoms with a cross-section that reaches its maximum value, 3×10^{-17} cm^2 at an energy of 120 eV. If the beam energy is less than E_{II} throughout the trap, production of Ar^{++} ions will be avoided. If this precaution is not taken, a small amount of the doubly charged species will be produced. This is common in mass spectrometers, as for example in residual gas analyzers, which typically produce ions using a 70 eV electron beam, and it is not important for some experiments. In some work with pure ion plasmas,[32] however, the impurity species produces significant complications. By dumping steady-state plasmas and measuring the time-of-flight spectrum, we have found that if the beam energy is substantially higher than E_{II} and $V>V_t$, the plasma consists predominantly of doubly ionized particles, which are preferentially confined. If $V<V_t$, the plasma is mostly singly charged particles. Time-of-flight spectra for these two different conditions are shown in Fig. 3. This change in character can easily be confused with another interesting phenomenon, which will be described below. To avoid these complications, the beam energy is kept below E_{II}. At these energies, the ionization cross section is about half of its maximum value.

The temperature of the ions is difficult to establish experimentally, due to the failure of the charge-dumping procedure (see Sec. IV A) upon which the magnetic beach temperature analyzer depends. The energy imparted to a gas atom during an ionizing collision with an electron is small, so that the initial ion energy distribution will range from 0 to qV, due to the quadrupole trap potential. Once significant space charge has accumulated and flattened the potential well, ions will be formed with a narrower range of energies. Collisions of ions with neutrals are expected to be mostly charge-exchange collisions, in which the ion removes an electron from a neutral with very little exchange of kinetic energy. The original ions are thus replaced by ions with the room-temperature energy distribution of the neutral gas. This strong cooling mechanism may be one reason that the frequencies of the azimuthal modes described in Sec. IV C are in good agreement with the cold fluid theory. The mean free path for charge-exchange of 10 eV Ar^+ ions in 1 μTorr of Ar is $\sim7\times10^3$ cm,[45] so that the mean time between collisions is of the order of 10 ms. This is fast compared to the confinement time for a single particle, but it is not clear how it compares to the confinement time of particles in the unusual plasmas described in the following section.

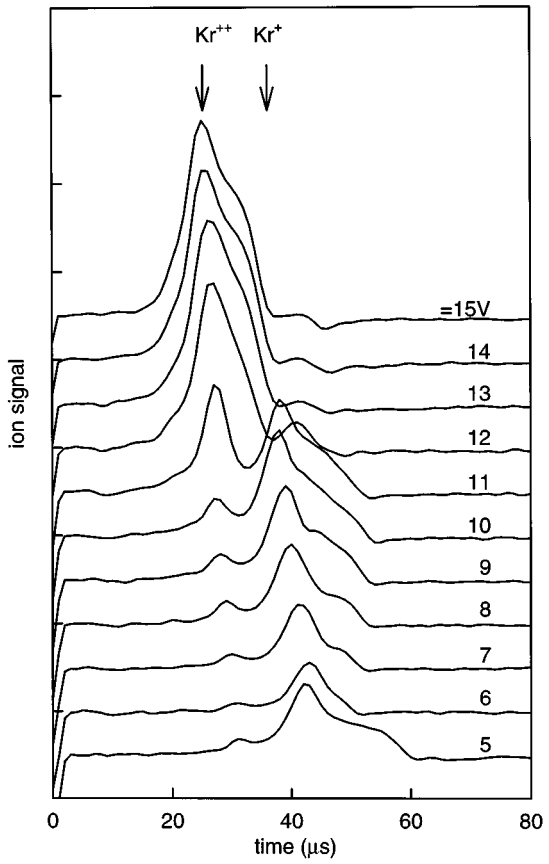

FIG. 3. Time-of-flight ion spectra showing transition from singly-ionized to doubly-ionized plasma as confinement voltage is increased.

IV. EXPERIMENTAL RESULTS

A. Total charge measurement

It would be desirable to measure the plasma profiles directly by dumping the plasma onto collector plates. There are two difficulties with this approach. The most fundamental problem is that if the plasmas are indeed near the Brillouin density, then the particles are not following magnetic field lines in the tight helices familiar from low-density electron plasmas. It is possible that during the dump the particles may become sufficiently magnetized to give some information. A problem specific to this experiment is that these large plasmas must be dumped through the moderate-sized hole in one of the endcaps. One might still hope to obtain data on the central portion of the plasma, but instead a sort of universal profile is obtained for all but the narrowest plasmas. Although the total charge received varies, the distribution is always strongly peaked in the center. This is consistent with a particle orbit radius comparable to or larger than the hole in the endcap, as is expected from the model. The difficulties with charge dumping also prevent us from measuring the plasma temperature.

Under some conditions, a measurement of the total plasma charge can be obtained by measuring the image charge flowing onto the confining electrodes as the trap fills. Because the filling is rapid (about 100 ms), a current spike is produced on the ring electrode when the electron beam is

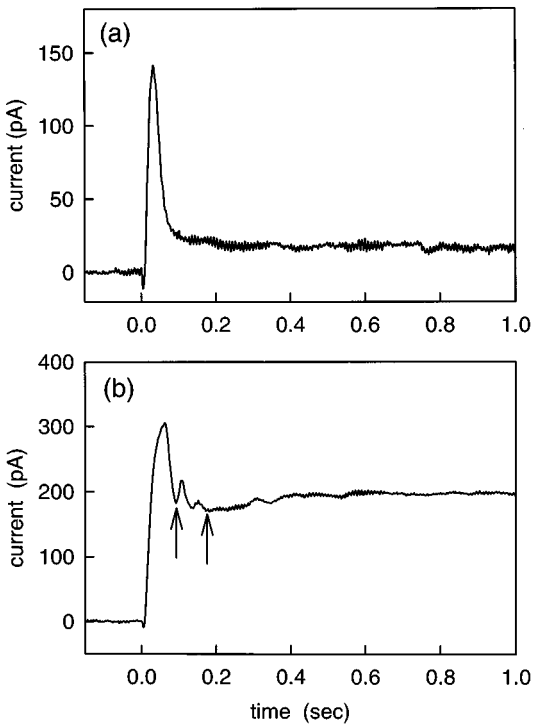

FIG. 4. Current transient to the ring electrode when electron beam is switched on at $t=0$, for an argon plasma with $B=1.31$ kG and (a) $V=5$ V; (b) $V=12.5$ V. The arrows indicate the integration end points corresponding to the bounds of the error bars in Fig. 5.

first switched on. For $V<V_t$, this spike is clearly distinguishable from the direct current (DC) which is established once the trap has been filled. Typical current traces, obtained using an electrometer, are shown in Fig. 4. The total charge is obtained by integrating the current spikes from all electrodes and correcting for the contribution from the image charge of the beam, which causes the small negative current spike seen at $t=0$. The measurement is unambiguous for small values of V, but as V approaches V_t, the current traces become more complicated, as shown in Fig. 4(b), making it difficult to decide when to stop the integration. The reason for these complicated features is not understood, but may be involved with the formation of a plasma sheath at either the endcaps or the ring electrode. For $V>V_t$, there is no clear separation between image charge current and the arrival of the steady-state current, and the technique is not applicable.

Figure 5 shows how the measured stored charge increases as V is increased. The error bars represent the uncertainty introduced by transient features of the sort shown in Fig. 4(b). The solid symbols represent the most plausible analysis. Using the model described in Sec. II D, the total charge in the Brillouin core is given by

$$Q=\frac{4}{3}\pi r_p^3 \alpha n_{\mathrm{B}}, \tag{16}$$

which is shown by the solid line in Fig. 5. The agreement between the data and the model is reasonably good, and at least verifies that the total charge is within about a factor of 2 of the model for $V<V_t$. This analysis ignores the halo of particles believed to surround the Brillouin spheroid. The

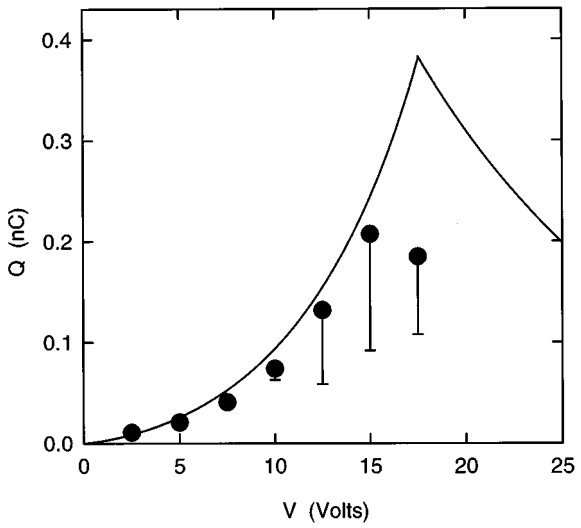

FIG. 5. Total charge of argon ion plasma with $B=1.31$ kG and various values of V. The solid line is from the steady-state model.

mode frequency data described in Sec. IV C suggests that this halo is not insubstantial, but we have no other information regarding it.

B. Transition in ring current

Less direct, but more convincing, evidence for the Brillouin spheroid model can be obtained by monitoring the steady-state current to the ring electrode. As may be seen in the transient current traces shown in Fig. 4, the steady-state current depends on V. It also depends on B, on the electron beam current, I_{beam}, and on the gas pressure, and all of the observed dependences are consistent with the model. In Fig. 6, the steady-state current to the ring is plotted as a function of V for various values of B and I_{beam}. In each case, the ring

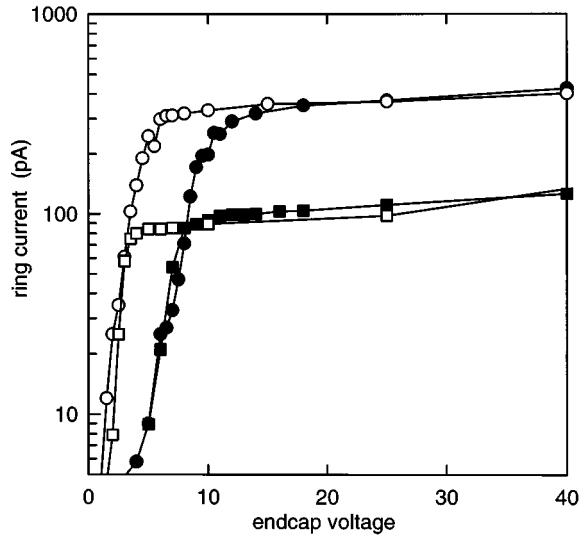

FIG. 6. Steady-state current to the ring electrode as a function of V for an argon plasma at a pressure of 2.4×10^{-8} Torr and with (□) $B=290$ G, $I_{\mathrm{beam}}=10$ μA; (○) $B=290$ G, $I_{\mathrm{beam}}=40$ μA; (■) $B=580$ G, $I_{\mathrm{beam}}=10$ μA; (●) $B=580$ G, $I_{\mathrm{beam}}=40$ μA.

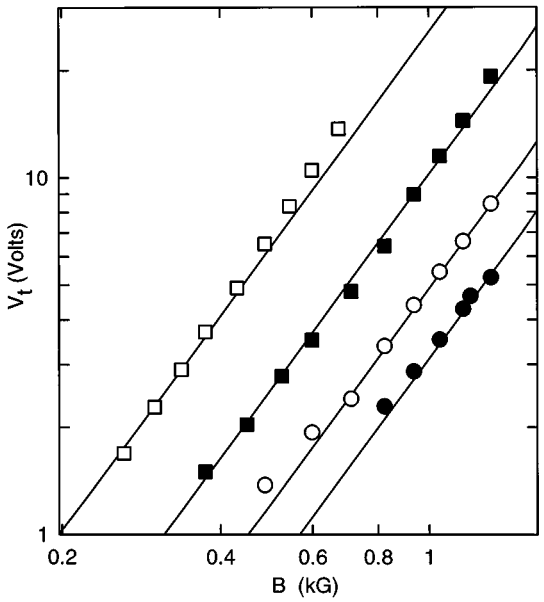

FIG. 7. Measured transition voltage as a function of B for four different ion species. (□) CH_4, (■) argon, (○) krypton, (●) xenon. Solid lines are from the model.

current is small for low values of V, corresponding in the model to the condition [Fig. 2(a)] in which the core plasma is not in contact with the ring, and most excess ions leave via the endcaps. The current increases steadily with V until a small jump occurs followed by a change in slope, presumably when $V \simeq V_t$ and the plasma contacts the ring [Fig. 2(b)]. The transition often shows substantial hysteresis, in which case the value obtained by approaching from lower values of V is recorded, since it matches the result obtained by dumping the plasma and refilling. The hysteresis may be associated with the formation of a plasma sheath when the ring is contacted. Further increases in V result in only slight increases in the ring current, which should now be the entire ion formation current. Comparing the different cases, we note that the value of B affects the value of V_t, but not the current for $V > V_t$. The beam current affects the ring current for $V > V_t$, as expected, but not for $V < V_t$. This is consistent with gas-scattering-induced radial current from the Brillouin core. As long as the ion formation rate is sufficient to keep the core filled, additional ions will leave through the endcaps, having no effect on the current to the ring. Finally, it is found that the ring current is approximately proportional to the gas pressure for all values of V. For $V > V_t$, this simply represents another way to get extra ion formation, which should add to the ring current. For $V < V_t$, the additional ions have no effect, but the rate at which ions scatter out of the core and migrate toward the ring is increased.

Because of the large hole in each endcap, most of the ion current that would flow to them for $V < V_t$ passes through the hole. The maximum endcap current is collected for $V \simeq V_t$, as expected, since these wide plasmas might be expected to make some contact with the endcaps.

Figure 7 shows the measured value of the transition voltage as a function of magnetic field for four ion species and the expected dependences, $V_t = (2 - \pi/2) V_c \sim B^2/M$, from the Brillouin spheroid model. No adjustable parameters were used. The excellent agreement seen in Fig. 7 between the model and the experiment was not obtained for plasmas made from He or H_2. We suspect that this reflects a combination of high n_B (due to low ionic mass) and low ionization cross-section compared to the cross-section relevant to radial transport, resulting in insufficient ion formation to balance losses.

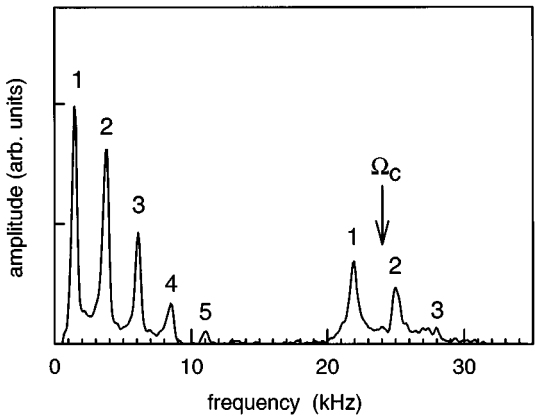

FIG. 8. Spectrum of azimuthal modes of an argon plasma, showing diocotron modes (0 to 10 kHz) and cyclotron modes (20 to 30 kHz). The numbers indicate experimentally determined values of m.

It was also found that for $I_{beam} > 10$ μA the measured values of V_t began to rise above the predictions of the model. An extra trapping effect from the field of the beam was considered (as in the Electron-Beam Ion Trap), but the presence of the beam electron density, n_e, should simply result in an increased local ion density, $n_i = n_B + n_e$, resulting in almost complete shielding of the beam. In any case, the beam current was kept low to avoid this effect.

C. Plasma modes

Plasma modes are excited by applying a signal to one of the sectors of the ring electrode and detecting the plasma response on another sector, as shown in Fig. 1. Frequency spectra are measured using a spectrum analyzer and a tracking generator. In the typical spectrum shown in Fig. 8, two families of modes are discernible. One family has frequencies near Ω_c. The lower-frequency family are the diocotron modes.[1] We note that for both families, the mode amplitudes decrease with increasing mode number, suggesting some k-dependent damping mechanism, possibly Landau damping, or a k-dependence in the excitation coefficient. The relatively large peak width does not appear to be an experimental artifact, but the reason for its origin is not clear at present.

A series of spectra like that shown in Fig. 8 were taken for steady-state argon plasmas for various values of V in the range $V_{min} < V \leqslant V_c$. Figure 9 displays the frequencies of the resonances observed as functions of V. A striking feature of the data is the discontinuity in the behavior of the modes that can be seen at $V = V_t$. The existence of this discontinuity is consistent with our model of the formation of a spheroidal core plasma at the Brillouin limit surrounded by a lower-density halo plasma. The discontinuity occurs at the precise

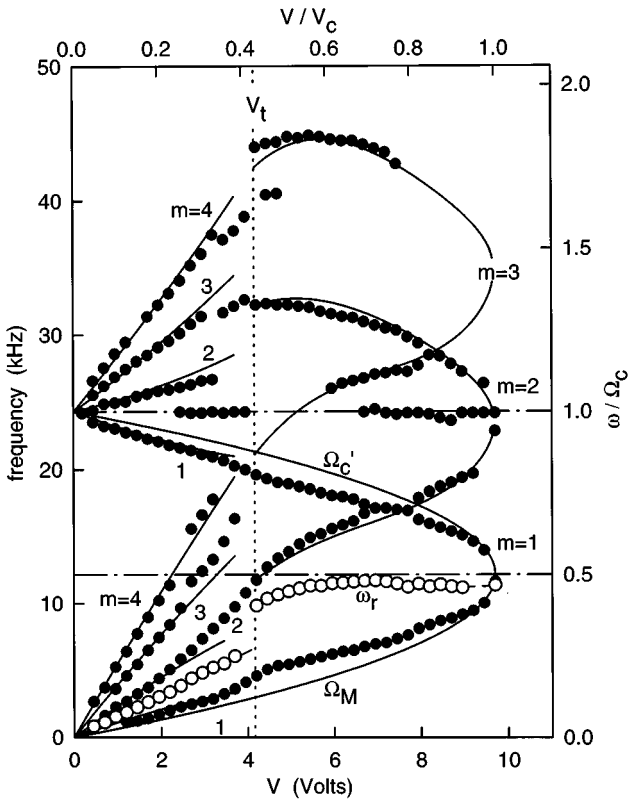

FIG. 9. Azimuthal mode frequencies of argon plasmas with $B=640$ G as functions of V. Values of m determined experimentally. Values of ω_r calculated from mode frequencies using Eq. (19). Solid lines obtained from the model are as described in the text.

voltage where the Brillouin core is predicted to contact the ring electrode, i.e., where the halo plasma is predicted to disappear. No fitted parameters are used in calculating V_t.

The cold fluid theory of spheroidal non-neutral plasma modes[36] predicts that modes of the form $\delta\Phi \sim e^{i(m\phi-\omega t)}$, which are expected to be excited by this technique, will have frequencies

$$\omega_m=(m-1)\omega_r+\frac{\Omega_c}{2}\pm\frac{1}{2}[(\Omega_c-2\omega_r)^2+2\omega_p^2 G_m(\alpha)]^{1/2}, \tag{17}$$

for positive m. The geometrical factor, G_m, is given by

$$G_m(\alpha)=2\left[m-\frac{Q_m^{m\prime}(k_2)}{\alpha(\alpha^2-1)^{1/2}Q_m^m(k_2)}\right]^{-1}, \tag{18}$$

where $k_2=\alpha(\alpha^2-1)^{-1/2}$ and the primes indicate differentiation with respect to the entire argument. The plus and minus signs in Eq. (17) give solutions ω_m^+ and ω_m^- corresponding to the cyclotron and diocotron branches of the dispersion relation, respectively. The plasma rotation frequency may be found from ω_m^+ and ω_m^- for any $m>1$:

$$\omega_r=\frac{\omega_m^+ + \omega_m^- - \Omega_c}{2m-2}. \tag{19}$$

These azimuthal ''flute'' modes are very similar to the analogous modes in a cylindrical single-component plasma. In the cylindrical case,[1] it is possible to include the effects of the image charge of the plasma. The mode frequencies again satisfy Eq. (17), with geometrical factors now depending on the ratio of the plasma radius, r_p, to r_w, the radius of the cylindrical wall, according to the relation $G_m(r_p)=1-(r_p/r_w)^{2m}$. If image charges are neglected in the cylindrical case by letting $r_w\to\infty$, the geometrical factors reduce to $G_m(r_p)=1$, and the mode frequencies match those of the $\alpha\to\infty$ limit of the spheroidal case, which did not include image charge effects.

We infer the rotation frequency of the plasma from the measured mode frequencies as follows. We first determine the azimuthal mode number m of each mode by applying a signal at the mode frequency to one of the electrodes, and then measuring the phase differences between the signals detected on several of the other electrodes. The measured values of m are indicated in Fig. 9. We next select pairs of cyclotron and diocotron modes with the same m values and apply Eq. (19). The open circles in Fig. 9 are the values of ω_r obtained by applying this procedure, using $m=2$, $m=3$, and $m=4$ modes for $V<V_t$ and the $m=2$ modes for $V>V_t$.

We first consider the modes for $V<V_t$. As shown in Fig. 9, the inferred rotation frequency (shown by open circles) is close to $2\Omega_M$, rather than $\Omega_c/2$, which would characterize a plasma at the Brillouin limit. For $V<V_t$, we expect the Brillouin core plasma to touch the endcaps, but to extend only part way out to the ring electrode. It would appear that the observed modes in this case are not supported by the Brillouin core plasma, but rather by a more tenuous surrounding plasma that forms a halo around the Brillouin core and shields it from the electrodes. Since this plasma is in contact with the ring electrode, it is reasonable that modes should be excited in this plasma rather than in the Brillouin core. Using these inferred rotation frequencies, we find that the frequency data may be fit to Eq. (17) by assuming $\omega_p^2 G_m=K_m\omega_z^2$, where $K_1=0.69$ and $K_m=1.24$ for $m>1$. These fit curves are the solid lines plotted for $V<V_t$ in Fig. 9. Also shown, for the whole range of V, are Ω_M and Ω_c', which should not depend on plasma parameters. The implications of this fit and of the observation that $\omega_r\simeq 2\Omega_M$ for the nature of the halo plasma are not understood at present.

Consider now the modes for $V>V_t$ shown in Fig. 9. The inferred rotation frequencies are only slightly below $\Omega_c/2$, which is the value that we would expect if the plasma were at the Brillouin limit. By substituting the measured rotation frequency into Eq. (5), we obtain values for ω_p^2, and hence n. This procedure gives values for n that vary from $0.96n_{\rm B}$ to greater than $0.99n_{\rm B}$ for all values of V above V_t. Knowing ω_p^2, we can also calculate α from Eq. (7), which then yields the mode frequencies predicted by the cold fluid theory from Eq. (17). The results are displayed in Fig. 9 as the solid lines shown for $V>V_t$. Except for the $m=1$ modes, the experimental data are in remarkably good agreement with the theory without using any fitted parameters. The discrepancy for the $m=1$ modes could result from the effects of image charge, which are not included in the model and which are expected to be most pronounced for modes with the lowest m-numbers.

Two nonlinear features of the data are the weak mode

observed near Ω_c, which is near the sum of the frequencies of the $m=1$ modes and could arise from these modes via quadratic coupling, and the mode coupling observed at the crossing of the $m=1$ cyclotron mode and the $m=2$ diocotron mode near $V=0.75V_c$.

V. DISCUSSION

We have developed a technique for producing steady-state plasmas at the Brillouin limit in a Penning trap by continuous ionization of a background gas using an electron beam. This technique produces spheroidal plasmas with density $n \simeq n_B$, and aspect ratio that depend on the confining voltage, V. For low values of V, the plasma is elongated and extends to the endcaps, while for V near the critical voltage, the plasmas are pancake-shaped and extend to the ring electrode. Plasmas with arbitrary aspect ratio can be obtained by selecting the appropriate confining voltage.

We have made the first direct measurements of azimuthally propagating modes in such a plasma. For V greater than some transition voltage, corresponding to the case where the plasma contacts both the ring and the endcaps (i.e., $\alpha=1/\sqrt{2}$), we have found that the modes can be described by the analytical cold-fluid model developed by Dubin.[36]

The remarkable simplicity of the steady state of these plasmas, the surprising degree to which the spheroidal mode theory is satisfied, and the apparently rich variety of phenomena that may be observed suggest that further experiments with similar systems are warranted. A pulsed beam could produce similar plasmas which do not touch the walls. The technique could be applied to the investigation of techniques that have been proposed for exceeding the Brillouin limit. For example, this method could be used to study the higher order magnetic multipole configurations in which the confinement limit has been predicted to exceed the Brillouin limit for a uniform magnetic field.[11] Another method of exceeding the Brillouin limit is by the excitation of plasma modes. One class of modes that is of particular interest are the so-called ''tilt'' modes, in which the $\vec{\omega}$ is parallel to the axial B-field, but the rotational frequency $\vec{\Lambda}$ of the fluid plasma with respect to the body axis is not. These solutions correspond to ellipsoids tilted with respect to the axial B-field, and precessing around it. For particular values of α, Ω_c, and ω_z, these ellipsoids are stationary in the laboratory frame, with a non-zero internal vorticity, giving rise to equilibria that exceed the Brillouin limit.[23] It should be possible to study such equilibria using the technique described in this paper, in a Penning trap with segmented endcap and ring electrodes, which would enable these modes to be studied.

In conclusion, it appears that creating and studying plasmas at the Brillouin limit is both interesting and relatively straightforward. This technique could be easily implemented in other devices, opening up the possibility of new insights into the unusual physics of the regime near the Brillouin limit.

ACKNOWLEDGMENTS

We are pleased to acknowledge helpful conversations with D. H. E. Dubin and the technical assistance of E. A. Jerzewski.

This work is supported by the Office of Naval Research.

[1] R. C. Davidson, *Physics of Nonneutral Plasmas* (Addison-Wesley, Redwood City, CA, 1990).
[2] T. M. O'Neil, in *Non-neutral Plasma Physics*, edited by C. W. Roberson and C. F. Driscoll (American Institute of Physics, New York, 1988), pp. 1–27.
[3] J. H. Malmberg, C. F. Driscoll, B. Beck, D. L. Eggleston, J. Fajans, K. Fine, X.-P. Huang, and A. W. Hyatt, in *Non-neutral Plasma Physics*, edited by C. W. Roberson and C. F. Driscoll (American Institute of Physics, New York, 1988), pp. 28–71.
[4] R. W. Gould, Phys. Plasmas **2**, 2151 (1995).
[5] L. Brillouin, Phys. Rev. **67**, 260 (1945).
[6] A. J. Theiss, R. A. Mahaffey, and A. W. Trivelpiece, Phys. Rev. Lett. **35**, 1436 (1975).
[7] G. Dimonte, Phys. Rev. Lett. **46**, 26 (1981).
[8] D. J. Heinzen, J. J. Bollinger, F. L. Moore, W. M. Itano, and D. J. Wineland, Phys. Rev. Lett. **66**, 2080 (1991).
[9] D. C. Barnes, R. A. Nebel, and L. Turner, Phys. Fluids B **5**, 3651 (1993).
[10] L. Turner and D. C. Barnes, Phys. Rev. Lett. **70**, 798 (1993).
[11] T. N. Tiouririne, L. Turner, and A. W. C. Lau, Phys. Rev. Lett. **72**, 1204 (1994).
[12] T. B. Mitchell, M. H. Holzscheiter, M. M. Schauer, D. W. Scudder, and D. C. Barnes, in *Non-Neutral Plasma Physics II*, edited by J. Fajans and D. H. E. Dubin (American Institute of Physics, New York, 1995), pp. 113–117.
[13] R. E. Pollock (private communication, 1994).
[14] H. W. Lefevre, R. C. Connolly, D. P. Xi, G. E. Sieger, and J. C. Overley, Nucl. Instrum. Methods B **10–11**, 707 (1985).
[15] D. J. Wineland, C. S. Weimer, and J. J. Bollinger, Hyperfine Interact. **76**, 115 (1993).
[16] M. M. Nieto and M. H. Holzscheiter, Appl. Phys. B (Lasers Opt.) **60**, 103 (1995).
[17] M. H. Holzscheiter, Hyperfine Interact. **81**, 71 (1993).
[18] G. Gabrielse, W. Jhe, D. Phillips, W. Quint, L. Haarsma, K. Abdullah, H. Kalinowsky, and J. Grobner, Hyperfine Interact. **81**, 5 (1993).
[19] M. Charlton, J. Eades, D. Horvath, R. J. Hughes, and C. Zimmermann, Phys. Rep. **241**, 65 (1994).
[20] J. J. Bollinger, D. J. Wineland, and D. H. E. Dubin, Phys. Plasmas **1**, 1403 (1994).
[21] A. W. Trivelpiece and R. W. Gould, J. Appl. Phys. **30**, 1784 (1959).
[22] J. H. Malmberg and J. S. de Grassie, Phys. Rev. Lett. **35**, 577 (1975).
[23] D. H. E. Dubin, Phys. Fluids B **5**, 295 (1993).
[24] K. S. Fine, C. F. Driscoll, and J. H. Malmberg, Phys. Rev. Lett. **63**, 2232 (1989).
[25] S. A. Prasad and J. H. Malmberg, Phys. Fluids **29**, 2196 (1986).
[26] W. D. White, J. H. Malmberg, and C. F. Driscoll, Phys. Rev. Lett. **49**, 1822 (1982).
[27] J. S. deGrassie and J. H. Malmberg, Phys. Rev. Lett. **39**, 1077 (1977).
[28] J. S. deGrassie and J. H. Malmberg, Phys. Fluids **23**, 63 (1980).
[29] C. F. Driscoll and K. S. Fine, Phys. Fluids B **2**, 1359 (1990).
[30] R. W. Gould and M. A. LaPointe, Phys. Rev. Lett. **67**, 3685 (1991).
[31] R. W. Gould and M. A. LaPointe, Phys. Fluids B **4**, 2038 (1992).
[32] E. Sarid, F. Anderegg, and C. F. Driscoll, Phys. Plasmas **2**, 2895 (1995).
[33] R. G. Greaves, M. D. Tinkle, and C. M. Surko, Phys. Rev. Lett. **74**, 90 (1995).
[34] M. D. Tinkle, ''Electrostatic oscillations of spheroidal single-component plasmas,'' Ph.D. thesis, University of California, San Diego, 1994.
[35] J. J. Bollinger, D. J. Heinzen, F. L. Moore, W. M. Itano, D. J. Wineland, and D. H. E. Dubin, Phys. Rev. A **48**, 525 (1993).
[36] D. H. E. Dubin, Phys. Rev. Lett. **66**, 2076 (1991).
[37] C. L. Wilkins, A. K. Chowdhury, L. M. Nuwaysir, and M. L. Coates, Mass Spectrom. Rev. **8**, 67 (1989).
[38] J. B. Jeffries, S. E. Barlow, and G. H. Dunn, Int. J. Mass Spectrom. Ion Proc. **54**, 169 (1983).

[39]C. S. Weimer, J. J. Bollinger, F. L. Moore, and D. J. Wineland, Phys. Rev. A **49**, 3842 (1994).
[40]M. D. Tinkle, R. G. Greaves, C. M. Surko, R. L. Spencer, and G. W. Mason, Phys. Rev. Lett. **72**, 352 (1994).
[41]C. M. Surko, M. Leventhal, and A. Passner, Phys. Rev. Lett. **62**, 901 (1989).
[42]R. G. Greaves, M. D. Tinkle, and C. M. Surko, Phys. Plasmas **1**, 1439 (1994).
[43]G. Gabrielse, L. Haarsma, and S. L. Rolston, Int. J. Mass Spectrom. Ion Proc. **88**, 319 (1989).
[44]L. Turner, Phys. Fluids **30**, 3196 (1987).
[45]S. C. Brown, *Basic Data of Plasma Physics* (Wiley, New York 1959).